Available online at www.sciencedirect.com
ScienceDirect
Polymer 49 (2008) 1651–1658
polymer
www.elsevier.com/locate/polymer

Viscoelastic electrospun jets: Initial stresses and elongational rheometry

Tao Han [a], Alexander L. Yarin [b], Darrell H. Reneker [a,*]

[a] Department of Polymer Science, The University of Akron, Akron, OH 44325-3909, United States
[b] Department of Mechanical and Industrial Engineering, University of Illinois at Chicago, Chicago, IL 60607-7022, United States

Received 11 October 2007; received in revised form 14 January 2008; accepted 17 January 2008
Available online 20 January 2008

Abstract

A novel method of characterization of viscoelastic longitudinal stresses in electrospun jets of semi-dilute and concentrated polymer solutions and melts is introduced. The measured longitudinal stresses at the beginning of the thin jet region in the jets of a 6 wt% aqueous solution of polyethylene oxide ($M_w = 400$ kDa) were of the order of 100 kPa, which is two orders of magnitude larger than in any other free viscoelastic jets issued from nozzles and orifices. This is attributed to elongation-driven stretching of polymeric liquids in the transition zone, between the preceding modified Taylor cone zone and the beginning of the thin jet region, where the stretching rates are of the order of 100–1000 s^{-1}. The Rouse relaxation times found were in the range of 3–8 ms, and the moduli of elasticity were of the order of 100 Pa. A novel explanation of the reasons for the formation of the straight sections in the electrospun jets is proposed. The straight sections are stabilized by the high initial longitudinal stresses in the jet generated due to strong electrically driven stretching in the transition zone. The further electrically driven stretching in the jet (after the transition zone) is relatively weak, and viscoelastic Rouse relaxation prevails. The relaxation distance of the longitudinal stresses along the jet increases with the applied voltage (which generates higher initial stresses in the transition zone) and thus the length of straight section of the jet should increase as the applied voltage increases.

The results also point at an opportunity to develop an elongational rheometer for concentrated polymeric systems with stretching rates of the order of 100–1000 s^{-1}. The proposed rheometer employs excitation of electrically driven jets by single lateral pulses, and observation of the pulse propagation and widening along the jet. This reveals the level of the longitudinal stresses along the jet and allows evaluation of the viscoelastic Rouse relaxation time, modulus of elasticity and the elongational viscosity in the jet.
© 2008 Elsevier Ltd. All rights reserved.

Keywords: Electrospinning; Elongational rheometer; Elongational stress

1. Introduction

Polymeric viscoelastic liquid jets represent key elements of technologies such as textile fiber spinning [1–4] and electrospinning [5–7] as well as in some other applications. Such jets can sustain significant longitudinal stresses of viscoelastic origin. In fiber spinning, aerodynamic jet bending, and electrospinning of viscoelastic liquids, both stretching and viscoelastic relaxation are present [1–7]. The longitudinal stress level is determined by the competition between the stretching and the relaxation. Three zones near the beginning of the jet are named as follows. The ''modified Taylor cone'' zone is nearest the orifice and is followed by the ''transition zone'', which is followed by the straight ''thin segment'' region. The shape of the static Taylor cone is modified by the flow of the solution and the electrical charge when the jet begins [7]. The static Taylor cone is not discussed elsewhere in this paper. Only the flow-affected ''modified Taylor cone'' is discussed.

In the electrically driven jets used for electrospinning, significant stretching of polymer solutions begins in the transition zone, between the modified Taylor cone, where the stress is small, and the beginning of the thin jet zone, where the liquid can already be significantly pre-stretched [8] (cf. Fig. 1). As a result of this pre-stretching, the electrically charged jet can possess a significant initial stress in the cross-section of diameter $2a_e$ (Fig. 1) which might affect its further evolution. The

* Corresponding author. Tel.: +1 330 972 6949; fax: +1 330 972 5461.
E-mail address: reneker@uakron.edu (D.H. Reneker).

0032-3861/$ - see front matter © 2008 Elsevier Ltd. All rights reserved.
doi:10.1016/j.polymer.2008.01.035

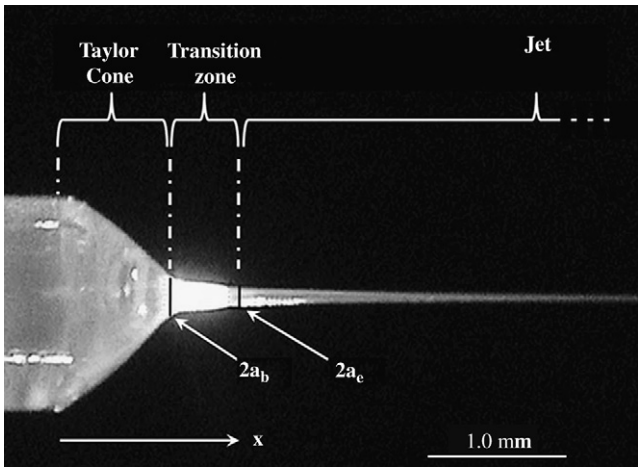

Fig. 1. Modified Taylor cone zone, with the transition zone, and the beginning of the thin jet in an electrically driven jet. The cross-sectional radii at the beginning and end of the transition zone are denoted a_b and a_e, respectively.

rate of strain in this strong and extremely short pre-stretching process in the transition zone is of the order of 100–1000 s^{-1} and can be estimated from the results of Ref. [8]. It will also be measured in the experimental part of this work (Section 4). Therefore, the viscoelastic jets can possess significant initial longitudinal viscoelastic stresses generated in the preceding flow domain (the transition zone). Moreover, the high longitudinal stresses in the jet affect its thinning, i.e. its shape. The shape changes affect the charge distribution at the jet surface, which has dramatic effects on the further evolution of the jet. In electrospinning of viscoelastic polymer solutions, the length of the initial straight part of the electrified jets is determined by the level of the longitudinal viscoelastic stresses [5] and electric forces. Mathematical descriptions of the diameter of a jet along its length in terms of the many parameters involved have been published [5,9–14]. Comparisons of the results from the various theoretical descriptions and experimental measurements reveal the complications and uncertainties. These uncertainties must be dealt with to make calculations that actually predict the shape of the straight electrified jet and to determine the viscoelastic parameters of concentrated polymer solutions and melts undergoing uniaxial elongation at extreme strain rates. Moreover, the role of non-zero initial stress in the jet which might arise from the pre-stretching in the transition zone has never been discussed or studied theoretically [5,7,9–14]. On the contrary, for the free viscoelastic liquid jets rapidly propagating in air and experiencing the aerodynamically driven bending instability, the crucial role of the initial viscoelastic stresses is well understood theoretically [4] and their level was measured in a number of experiments [15–18]. In particular, the method of periodic transverse vibrations was proposed which allows measurement of the level of the longitudinal stresses in uncharged jets freely moving in air as well as an estimate of the viscoelastic Rouse relaxation time of the liquids in such jets [15–19]. The aim of the present work is to develop a novel measurement method based on the analysis of a single lateral pulse imposed on a jet, as sketched in Fig. 2. Such a pulse is created as a bending

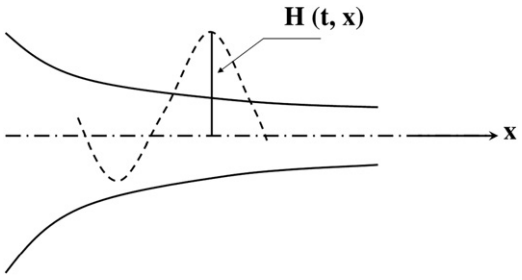

Fig. 2. Sketch of a tapered straight jet and lateral bending perturbation of its axis. The detailed shape of perturbation pulse is not critical, as long as the locations of two or more recognizable features such as extremal points or zero crossings can be followed.

perturbation imposed by a lateral impactor for example. The pulse begins to propagate along the jet (it is swept by flow and in addition possesses its own propagation velocity relative to the fluid). During its motion, the pulse widens. Widening was employed for measurements of longitudinal viscoelastic stresses and the Rouse relaxation time in the electrically driven jets characteristic of electrospinning. In particular, this paper describes the way to measure the velocity of the fluid in the jet everywhere along the length of the jet, from the observed diameter of the jet as a function of position along the jet and the laser Doppler velocimeter data at at least one point. The paper also describes the experimental measurement of the tensile stress in the jet by creating a lateral displacement of a short segment near the beginning of the jet and observing the propagation of the displaced segment along the jet. Such an experiment provides the information needed to measure the tensile stress as a function of position along the jet path. Combination of the observed fluid velocity data with the observed stress data at each point provides the information needed to determine the modulus of elasticity and the Rouse relaxation time of a polymeric liquid subjected to an extremely strong stretching. Suitable experimental observations were made in the transition zone and the straight segment of a straight electrified jet, as defined in Fig. 1.

Section 2 describes the theoretical background for this novel method. In Section 3 the experimental setup and materials used are presented. Section 4 contains the experimental results and discussion. Conclusions are drawn in Section 5.

2. Theoretical background

In a typical electrospinning device for the manufacture of nanofibers, a steady state shape of the jet along its path is established when distance between the electrodes is kept short (not more than several centimeters). To create a jet with a steady shape, the geometry of the orifice and the fluid pressure inside the orifice were held constant. A particular viscoelastic solution was used, and a particular electrical potential distribution between the orifice and the collector was established. All other spinning conditions were also maintained during the measurements. The diameter of the jet can be observed and measured as a function of the position along the path.

Due to the mass conservation in the transition zone (practically no solvent evaporation has yet occurred), the elongation of a material element there is $\lambda = (a_b/a_e)^2$, where a_b and a_e are the cross-sectional radii at the beginning and end of the transition zone. It is well-known that polymer solutions react to strong and almost instantaneous stretching almost as an elastic neo-Hookean (rubber-like) body with practically no relaxation involved [4]. The stress σ_{xxe} at the end of the transition zone (the initial stress in the thin jet) is then given by

$$\sigma_{xxe} = 2G\lambda^2 = 2G\left(\frac{a_b}{a_e}\right)^4 \tag{1}$$

where G is the modulus of elasticity and a_b and a_e are measured from the photographs of the transition zone (Fig. 1). The viscoelastic relaxation is neglected in Eq. (1), since it is expected (and proved a posteriori in Section 4) that the residence time of fluid elements in the transition zone t_r is shorter than the Rouse relaxation time θ.

Consider now an initial straight tapering section of an electrically driven viscoelastic jet of polymer solution moving in air (the thin jet with the cross-sectional radii less than a_e in Fig. 1). This may be a jet traveling a short inter-electrode distance of the order of 1 cm, a distance too short for a bending instability to develop, or the straight section of an electrospinning jet, preceding the loops of the bending instability [5–7]. The electric force acting on the jet section is longitudinal, and even if the straight section were forced to bend by an impactor, the resulting lateral electric force would still be much less than the longitudinal viscoelastic force established by the high electrical charge density in the jet cross-section and over its surface [5–7]. When bending perturbations are imposed on a straight jet or its straight initial section in electrospinning, the perturbations are assumed to be sufficiently small. They are also assumed to be planar. Based on the momentless quasi-one-dimensional equations of the dynamics of free liquid jets [4,20], it is easy to show that the normal projection of the momentum balance equation (4.19) in p. 49 in Ref. [4] takes the following form

$$\frac{\partial^2 H}{\partial t^2} + 2V(x)\frac{\partial^2 H}{\partial t \partial x} + \left[V(x)^2 - \sigma_{xx}(x)/\rho\right] = 0 \tag{2}$$

where t is the time, x is the longitudinal Cartesian coordinate along the unperturbed jet axis, $H = H(t,x)$ is the normal displacement of the jet axis (cf. Fig. 2), $V = V(x)$ is an unperturbed distribution of the longitudinal liquid velocity along the jet, $\sigma_{xx} = \sigma_{xx}(x)$ is an unperturbed tensile stress in the jet cross-section, and ρ is the liquid density.

The hyperbolic Eq. (2) describes the propagation of sufficiently small bending perturbations along a straight tapering viscoelastic jet. It was also derived as Eq. (2) in Ref. [17], however, its general solution relevant for pulse propagation was not considered there or in the other related works. Note that the normal (lateral) velocity of the jet related to bending perturbations is given by $V_n = \partial H/\partial t$.

The hyperbolic Eq. (2) possesses two characteristics

$$\xi(t,x) = \int_0^x \frac{dx}{V + \sqrt{\sigma_{xx}/\rho}} - t = C_1 \tag{3}$$

$$\eta(t,x) = \int_0^x \frac{dx}{V - \sqrt{\sigma_{xx}/\rho}} - t = C_2 \tag{4}$$

where C_1 and C_2 are constants. Therefore, the general solution of Eq. (2) is given by

$$H(t,x) = \Phi\left(\int_0^x \frac{dx}{V + \sqrt{\sigma_{xx}/\rho}} - t\right) + F\left(\int_0^x \frac{dx}{V - \sqrt{\sigma_{xx}/\rho}} - t\right) \tag{5}$$

where $\Phi = \Phi(\cdot)$ and $F = F(\cdot)$ are arbitrary functions. For any particular perturbation pattern (e.g., time-periodic perturbations or a single pulse) these functions can be always found via the initial conditions, namely

$$H = H_0(x) \quad \text{at } t = 0; \; V_n = \frac{\partial H}{\partial t} = V_{n0}(x) \quad \text{at } t = 0 \tag{6}$$

where the initial wave pattern $H_0(x)$ and the lateral velocity distribution related to it $V_{n0}(x)$ can be, in principle, measured experimentally. The longitudinal velocity distribution in the unperturbed jet is also known in principle as $V(x) = Q/[\pi a(x)^2]$, where Q is the volumetric flow rate and the cross-sectional radius distribution $a = a(x)$ (with $a \le a_e$) can be measured experimentally or calculated using the existing theoretical models [4–7]. The unperturbed tensile stress distribution $\sigma_{xx}(x)$ along the jet is not immediately measurable, and our aim is to establish it using the above results.

Determination of $\sigma_{xx}(x)$ does not require knowledge of $V(x)$ (or $a(x)$) and $V_{n0}(x)$. The solution of Eq. (5) represents a superposition of two d'Alembert waves (signals) Φ and F, which propagate with speeds $V + \sqrt{\sigma_{xx}/\rho}$ and $V - \sqrt{\sigma_{xx}/\rho}$, respectively. Any pulse-like perturbation widens by $2\sqrt{\sigma_{xx}/\rho}\Delta t$ during time Δt, since it is propagated by the two signals. The widening of the pulse W between $t = 0$ and $t = \Delta t$ can be measured. Then

$$\sigma_{xx} = \rho\left(\frac{W}{2\Delta t}\right)^2 \tag{7}$$

Two cases (i) and (ii) are considered; (i) by repeating the experiment with the pulse being applied at different coordinates x, one can, in principle, measure the whole profile of the unperturbed stress $\sigma_{xx}(x)$ along the jet. (ii) If the duration of the pulse observation time Δt is taken much less than the shortest expected relaxation time (say, Δt is taken of the order of 0.5 ms), one can avoid the necessity for applying multiple pulse application at different locations x.

In case (ii), observing a single pulse propagating along the whole jet, we can consider it as different pulses applied at

different locations, while the local observation time Δt is taken short enough that the elastic relaxation time characteristic of stress σ_{xx} in an observed jet segment will be longer than the observation period from t to $t + \Delta t$. Then, the measured value of W and thus σ_{xx} could be attributed to the location of the pulse peak between t and $t + \Delta t$. The experimental procedure based on observations of a single pulse case (ii) was implemented in the present work.

3. Experimental

3.1. Materials

Polyethylene oxide, PEO ($M_w = 400$ kDa), purchased from Scientific Polymer Products, Inc., was used as a 6 wt% solution in water. Density of the solution was 10^3 kg/m^3, zero shear viscosity was 5 Pa s, surface tension was 61 mN/m, and the electrical conductivity was 0.0125 S/m. The experiments were done under ambient conditions at room temperature and relative humidity of about 25%.

3.2. Experimental setups

A digital video camera attached to an optical microscope was used to record the profile of the transition zone between the modified Taylor cone and the beginning of the jet (see the sketch in Fig. 3). The experiment was conducted as follows. Polymer solutions were held in a glass pipette which had tip several centimeters long with an 800 μm inner diameter. A copper wire was immersed in the solution and connected with a high voltage power supply which generated DC voltage up to 13 kV. A grounded horizontal plate was placed below the pipette tip to serve as a collector electrode. The distance between the pipette tip and the grounded plate could be adjusted from 0.1 cm to 30 cm. An ammeter was connected between the collector plate and the ground to measure the current carried by the electrically driven jet.

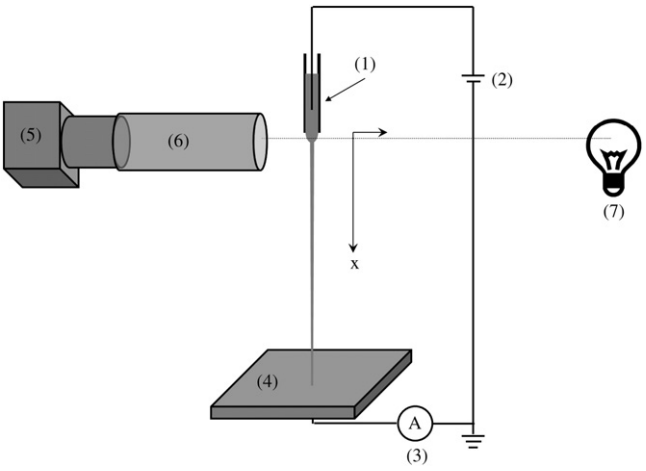

Fig. 3. Schematic drawing of the experimental setup for measuring radius and velocity distributions and evaluating the stretching rate. (1) Pipette; (2) high voltage DC power supply; (3) ammeter; (4) grounded collector; (5) digital video camera; (6) optical microscopy; (7) illumination light.

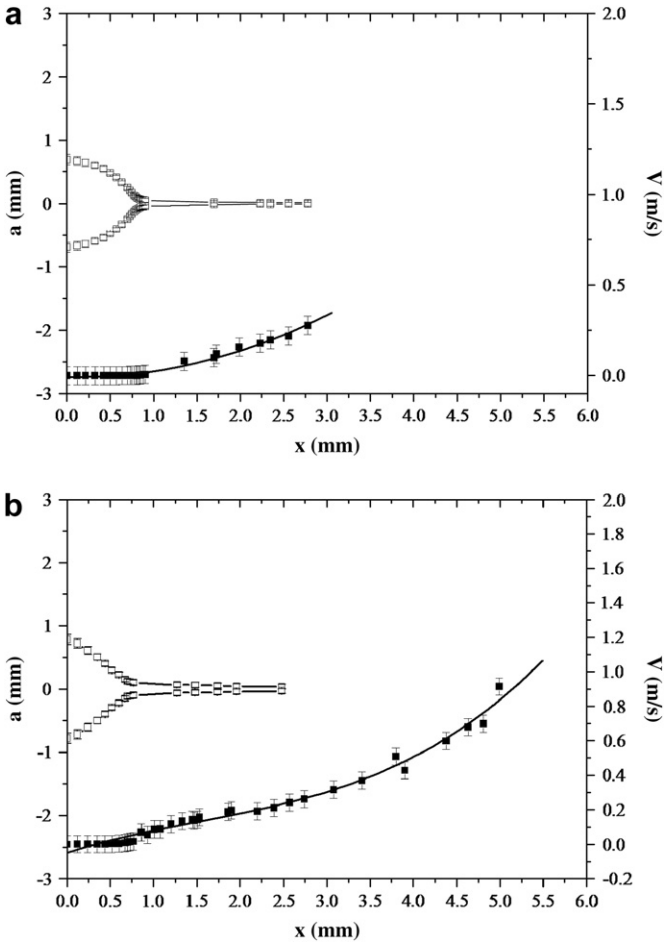

Fig. 4. Profile of the transition zone following the modified Taylor cone and the beginning of the jet. The cross-sectional radius is shown as $a = a(x)$ (the symmetric profile in the middle-left), where the axial coordinate x is zero at the first observable cross-section of the drop. At the end of the transition zone and the beginning of the thin jet, $x = x_e$ and $a = a_e$, respectively. The velocity distribution measured is shown by the solid curve below the profile $a = a(x)$. The change in the jet diameter after the transition zone is practically unseen in this scale which is the reason that the velocity distribution in the figure in (b) extends beyond the profile of the transition zone. The applied voltage was 3 kV in (a) and 5 kV in (b).

The cross-sectional radius in the transition zone $a = a(x)$ ($a_e \le a \le a_b$ in Fig. 1) was measured from the images of the transition zone (Fig. 4). Then, the longitudinal velocity $V = V(x)$ was calculated as $V = Q/(\pi a^2)$ where Q is the volumetric flow rate sustained in the experiment. A laser Doppler velocimeter was used to measure the velocity of the thin jet following the transition zone (where $a \le a_e$). The velocity profiles in the transition zone and the jet were combined and matched each other smoothly (Fig. 4). Similar trends were elucidated in the voltage range 3–5 kV.

The single-pulse experiment was conducted as follows. A bar of foamed polystyrene with a high stiffness and low density was glued onto a loudspeaker which produced a single lateral displacement pulse when a suitable electrical pulse was applied. The bar was positioned as shown in Fig. 5 so that the displacement pulse from the loudspeaker imparted a pulse-like lateral motion to the tip of the pipette. The amplitude of the lateral motion of the tip was about 2 mm. The time from the beginning to the end of the pulse was about 4–5 ms.

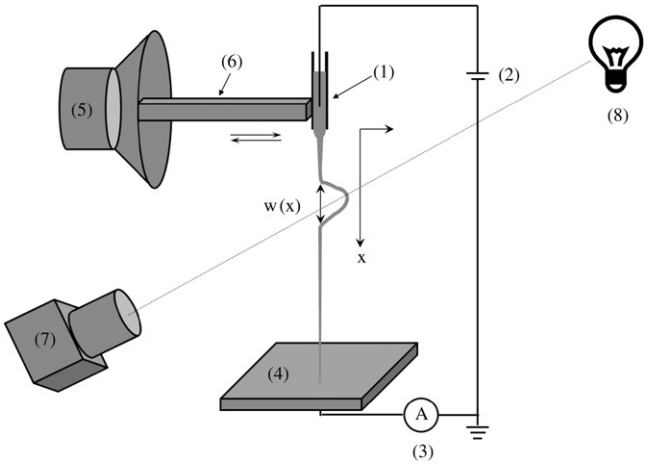

Fig. 5. Schematic drawing of the experimental setup for measuring longitudinal stresses in jets. (1) Pipette; (2) high voltage DC power supply; (3) ammeter; (4) grounded collector; (5) loudspeaker; (6) polystyrene bar; (7) high-speed camera; (8) illumination light. The viewing direction of the camera was perpendicular to both the displacement direction and the jet axis.

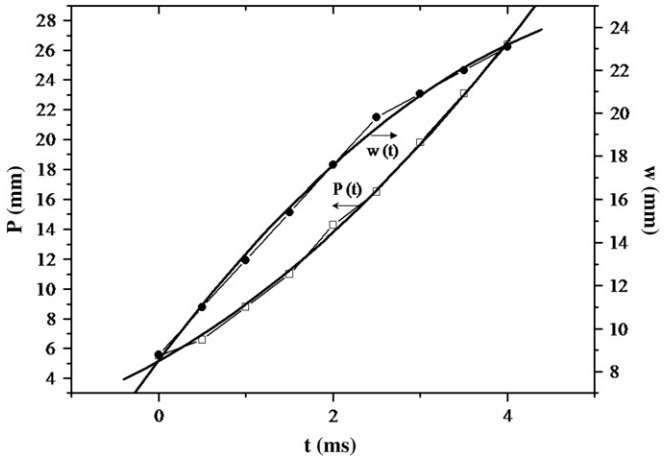

Fig. 7. Pulse peak location P and width w versus time. The broken lines connect the data points shown by symbols, and the smooth lines show the best fit of the data. The width versus time curve was used to evaluate $\partial w/\partial t = W/\Delta t$, needed to calculate the longitudinal stress σ_{xx} in the unperturbed jet using Eq. (7). The voltage applied to issue the jet was 3 kV in this case.

4. Results and discussion

The stretching rate in the transition zone is equal to dV/dx. Its values were found using the data shown in Fig. 4 and were in the range 100–1000 s^{-1}. This is a tremendously high rate of strain, for 6 wt% polymer solutions, which is not achieved in other experiments.

Image of the pulse propagation and widening images is presented in Fig. 6 for the applied voltages in the range $U = 3$–5 kV. The images show similar trends at $U = 3$ kV and 5 kV. The images in Fig. 6 were used to determine the location of the pulse peak, P, and the width, w, versus time. The peak positions and the width of the pulse were measured at intervals of 0.5 ms. The observations of a single peak propagating along the jet were used to acquire information for the entire length of the jet, as discussed in case (ii) in Section 2. An example of such processing is shown in Fig. 7. Data for $w(t)$ was approximated by a smooth function shown in Fig. 7 as a solid line. It was possible to differentiate w(t) and find the derivative $\partial w/\partial t$ corresponding to any instantaneous location of the

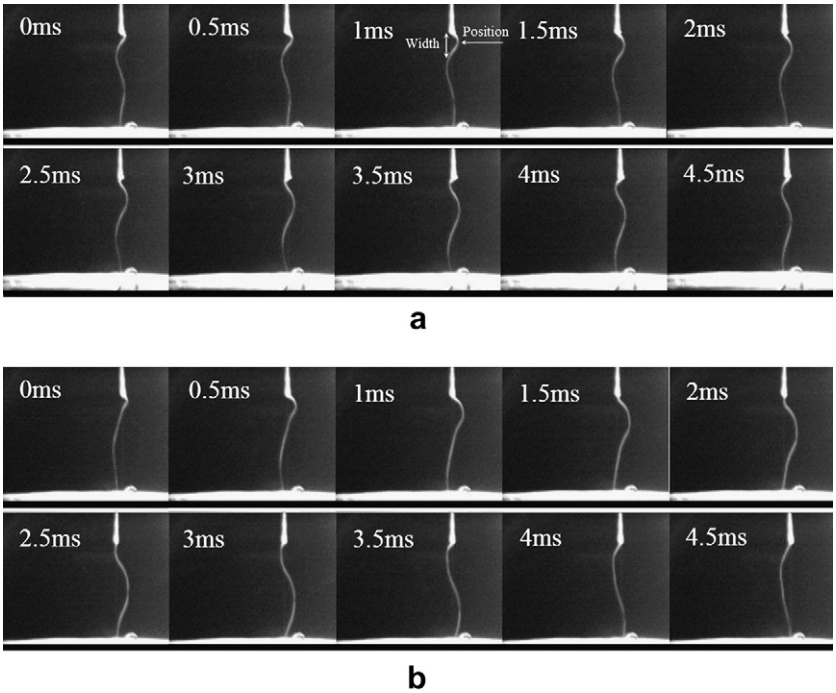

Fig. 6. Propagation and widening of a single lateral displacement pulse. (a) The inter-electrode distance $L = 5.5$ cm, potential difference of $U = 3$ kV, and the electric current $I = 100$ nA. (b) The inter-electrode distance $L = 5.5$ cm, potential difference of $U = 5$ kV, and the electric current $I = 880$ nA. In all the cases the jet was straight before the lateral displacement pulse was applied.

lateral displacement pulse propagating over the whole jet. The data shown in Fig. 7 were used to calculate the widening rate of the pulse at different locations along the jet. It was possible to calculate the pulse widening over time intervals much shorter than any expected relaxation time value. Using $W/\Delta t = \partial w/\partial t$, the stress σ_{xx} in the unperturbed jet was calculated via Eq. (7).

The value of σ_{xx} thus found can be associated with either the value of t used to calculate the derivative $\partial w/\partial t = W/\Delta t$ or the corresponding peak location $P = P(t) = x$. Thus, $\sigma_{xx} = \sigma_{xx}(t)$ can be recast into $\sigma_{xx} = \sigma_{xx}(x)$. These graphs are presented in Fig. 8.

It takes a longer time t_m for a material element of the jet near the lateral pulse to reach a location x, than is required for the pulse, moving along the jet, to reach the same location. The time t_m is given by the equation

$$t_m = \int_0^x \frac{dx}{V(x)} \tag{8}$$

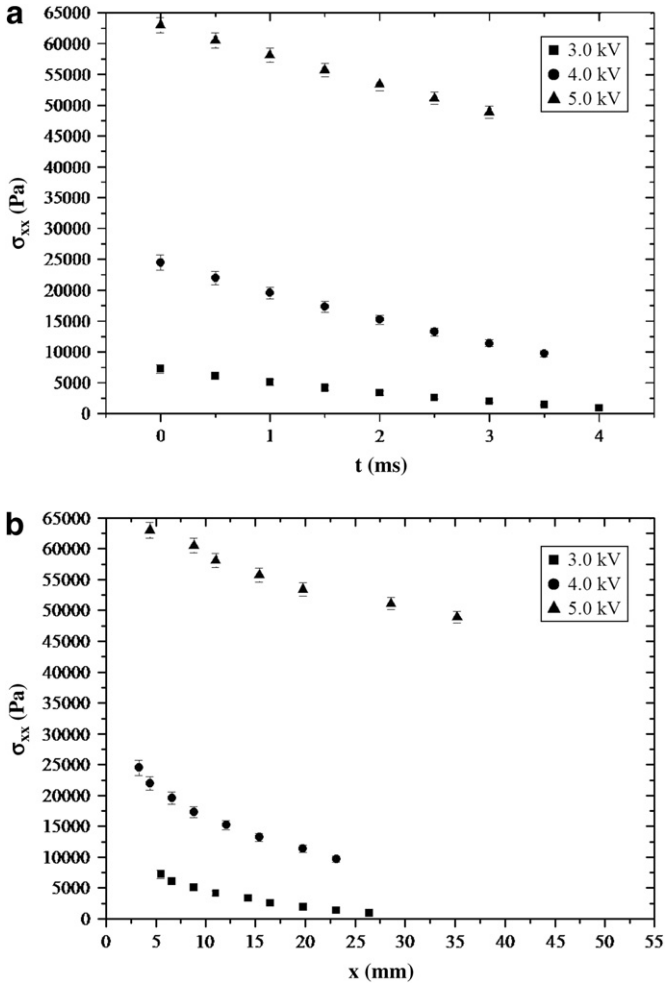

Fig. 8. Longitudinal stress distribution over the straight unperturbed electrified jet for different applied voltages. The inter-electrode distance was held at 5.5 cm. (a) Stress versus pulse-related time t, $\sigma_{xx} = \sigma_{xx}(t)$. (b) The Eulerian presentation as $\sigma_{xx} = \sigma_{xx}(x)$. Symbols show the experimental data for different applied voltages. The first points on the left correspond to the end of the transition zone and the beginning of the thin jet at $x = x_e \approx 2$–5 mm, where x is measured from the first observable cross-section of the drop as shown in Figs. 1 and 4.

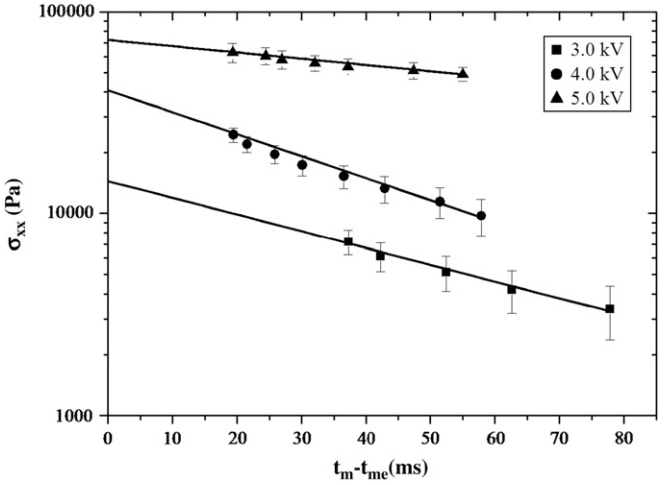

Fig. 9. The Lagrangian presentation of the stress as a function of time, $\sigma_{xx} = \sigma_{xx}(t_m - t_{me})$. The time moments when the material element exits the transition zone and reaches the beginning of the thin jet are denoted by t_{me}. The values of t_{me} were 15,145 ms, 1880 ms and 1183 ms for the voltages of 3 kV, 4 kV and 5 kV, respectively. The distributions of stress σ_{xx} versus $t_m - t_{me}$ are plotted in semi-logarithmic scale. Symbols show the experimental data for different applied voltages; lines are plotted using Eqs. (9) and (10).

Then, the stress distribution $\sigma_{xx}(x)$ (in the Eulerian sense) can be recast into $\sigma_{xx}(t_m)$ (in the Lagrangian sense), as shown in Fig. 9.

The initial stresses at the beginning of the thin jets appeared to be of the order of 10–100 kPa (the first points in the left in Figs. 8 and 9). The latter value is larger than those reported for the uncharged jets [16–18] by two orders of magnitude. This reveals the strong electrical forces affecting polymer solutions in the transition zone prior to the formation of a thin jet. The higher the applied voltage is (at a fixed inter-electrode distance), the higher is the value of the longitudinal stress generated near the beginning of the thin jets. Figs. 8 and 9 show that relaxation effects in the straight, thin jets dominate the stretching effect of the electric stresses acting on them, which means that the flow is weak there, following the terminology used in polymer rheology. Therefore, the longitudinal stresses relax along the jet. This result invalidates many theoretical models of the straight part of the viscoelastic electrospinning jets published so far, since such models disregard the existence of these high initial longitudinal stresses generated in the transition zone between the Taylor cone and the beginning of the jet. Moreover, the results in Ref. [4] (in particular, in Fig. 3.25 in p. 141) show that growth of bending perturbations is delayed by the initial high longitudinal stresses in the transition zone of the jets. Even though this result was first found, in Ref. [4], for the aerodynamically driven bending instability, it can be immediately recast for the electrically driven bending instability, since the equivalence of the two phenomena was established [6]. This equivalence allows the following interpretation of the results presented in Figs. 8 and 9: the electrically driven bending instability is impossible from the tip of the modified Taylor cone up to distances of about 2–4 cm along the jet, because the stabilizing longitudinal stresses there are sufficiently high. This indeed happens [5–7]. Moreover, the results depicted in Figs. 8 and 9 suggest that the straight

section of an electrospun jet should be longer if the jet is formed at a higher applied voltage. Again, the predicted increase in the length of the straight segment of the jet with an increase in the applied voltage is seen in experiments [5–7].

The initial longitudinal stress σ_{xxe} should be attributed to $t_m - t_{me} = 0$ (i.e. to $x = x_e$) in each experiment depicted in Fig. 9. The values of t_{me} for these experiments are listed in the caption of Fig. 9. It is emphasized that the values of t_{me} incorporate all the prehistory of the fluid elements (at $0 \le x \le x_e$) as the elements moved from the very beginning of the modified Taylor cone where the flow is extremely slow and the residence time is large. That is the reason that the values of t_{me} (and t_m) are of the order of 10^3–10^4 ms. Then, fitting of Eq. (1), with a_b and a_e being measured from the images similar to that in Fig. 1, reveals the corresponding values of the modulus of elasticity G. It was found that $G = 53.26$ Pa, 163.3 Pa and 395.4 Pa for the applied voltages of 3.0 kV, 4.0 kV and 5.0 kV, respectively. Stress relaxation in a material liquid element moving along the jet seen in Fig. 9 can be interpreted using an expression derived by the integration of the equations of the Upper-Convected Maxwell (UCM) model with a single relaxation time

$$\sigma_{xx} = \sigma_{xxe} \exp\left[-(t_m - t_{me})/\theta_{eff}\right] \tag{9}$$

$$\theta = \frac{\theta_{eff}}{1 + 2(dV/dx)_{max}\theta_{eff}} \tag{10}$$

where θ_{eff} is the effective relaxation time; θ is the Rouse relaxation time corresponding to contraction of macromolecules to their equilibrium length [4,21]; $(dV/dx)_{max}$ is taken as the largest positive value of the stretching rate. Fitting Eqs. (9) and (10) to the experimental data shown in Fig. 9, one can find σ_{xxe} and θ (shown in Table 1). Therefore, both characteristic rheological parameters of polymer solutions, G and θ, can be established in one experiment using Eqs. (1), (9) and (10) (Table 1). The initial elongational viscosity in the jet is then estimated as $\mu_\ell = \sigma_{xxe}\theta$ (Table 1).

Eqs. (9) and (10) follow from the integration of the following rheological constitutive equations of the UCM model

$$\frac{d\tau_{xx}}{dt_m} = \left(2\frac{dV}{dx} - \frac{1}{\theta}\right)\tau_{xx} + 2\frac{\mu}{\theta}\frac{dV}{dx} \tag{11}$$

$$\frac{d\tau_{yy}}{dt_m} = -\left(\frac{dV}{dx} + \frac{1}{\theta}\right)\tau_{yy} - \frac{\mu}{\theta}\frac{dV}{dx} \tag{12}$$

valid for uniaxial elongation in a jet [4,21], where μ is zero-shear viscosity, and τ_{xx} and τ_{yy} are the longitudinal and lateral deviatoric stresses in the jet, while the longitudinal stress $\sigma_{xx} = \tau_{xx} - \tau_{yy}$. The initial conditions are: $t = t_{me}$, $\tau_{xx} = \tau_{xxe}$, $\tau_{yy} = \tau_{yye}$ (and thus $\sigma_{xx} = \sigma_{xxe} = \tau_{xxe} - \tau_{yye}$). The integration leading to Eqs. (9) and (10) is done for $dV/dx = (dV/dx)_{max} = \text{const}$. The result shows, as expected in jets, that $\tau_{xx} \gg \tau_{yy}$, and thus $\sigma_{xx} \approx \tau_{xx} \approx \sigma_{xxe}\exp\{-[1/\theta - 2(dV/dx)_{max}](t_m - t_{me})\}$. The fact that the experimental data show that the stress σ_{xx} decreases when a material element moves along the jet means that in the present case the viscoelastic relaxation reduces the tensile stress faster than the elongation due to the electric field increases the stress, and thus $1/\theta > 2(dV/dx)_{max}$. In this sense, the flow in the straight thin part of the jet is weak, whereas the flow in the preceding transition zone is strong, since it results in a build-up of the longitudinal stress. It is emphasized that Eqs. (9) and (10) account for the jet stretching by the electric field which determines the value of $(dV/dx)_{max}$. In a more detailed analysis, the integration of Eqs. (11) and (12) could be modified to include the fact that dV/dx could vary along the jet. This modification could be made in the framework of a conjugate problem, incorporating the quasi-one-dimensional equations of the mass and momentum balance for jets, the rheological constitutive Eqs. (11) and (12) and the electric field description accounting for the interaction of the surface charges on the jet with the electric field. Examples of numerical solutions of similar conjugate problems can be found in Refs. [9,10] although these examples do not include the accounting for the initial stresses. In the present work we avoid dealing with the conjugate problem and detailed calculation of the electric field about the jet, because we use the experimental velocity data for $V(x)$ to evaluate dV/dx. Since the experimental data obviously reflect the effects of the electric field via $V(x)$, the parameter values obtained and presented in Table 1 are affected by the electric field properly, with no need for further calculation.

Table 1
Characteristics of the polyethylene oxide solution calculated from Eqs. (1), (9) and (10)

U (kV)	σ_{xxe} (Pa)	G (Pa)	θ (ms)	μ_ℓ (Pa s)
3.0	14,431	53	8.3	119
4.0	26,455	163	3.0	80
5.0	64,050	395	3.0	190

The Rouse relaxation times found are in the range $\theta = 3$–8 ms (Table 1). The residence time in the transition zone is of the order of $t_r \approx (0.5 \times 10^{-1}\ \text{cm})/(0.5 \times 10^2\ \text{cm/s}) \approx 1$ ms (cf. Figs. 1 and 4). Therefore, the assumption $t_r < \theta$ holds indeed, and the relaxation effects in the transition zone can be neglected, as it was done in Eq. (1).

It is worth emphasizing that electrospinning jets consist of the three distinct zones discussed above in addition to one or more electrically driven bending zones. In order along the jet these are: (1) a modified Taylor cone (a very weak, almost Newtonian flow), (2) a transition zone (a strong elongational flow at rates of 100–1000 s^{-1}), (3) a straight thin jet (a weak elongational flow at a strain rate averaged over the entire length of the straight segment that is of the order of 20 s^{-1}, [5]), and (4) bending loops (with an initial strong elongational flow with strain rates of the order of 1000 s^{-1} which decrease rapidly with length [5]).

Stretching in the transition zone is very strong (at the rates of 100–1000 s^{-1}). Therefore, the method outlined here can be used for the elongational rheometry of concentrated polymer solutions and melts under the conditions of an extremely strong elongation. We are unaware of any other method which could be used for elongational measurements of concentrated polymer systems with such high rates of strain.

5. Conclusion

A novel method of measurement of viscoelastic longitudinal stresses in straight electrically driven jets of polymer solutions is proposed and applied to jets characteristic of electrospinning. The method is based on the observation of propagation of a single lateral pulse imposed on the jet and of the profile of the unperturbed jet. The results revealed that the initial longitudinal stress created by the electric stretching of the jet as it transforms from the modified Taylor cone to a thin jet is of the order of 10–100 kPa. These values are one or two orders of magnitude larger than those measured for uncharged viscoelastic jets. This shows that stretching of polymer solutions in the transition zone of the electrically driven jets following the modified Taylor cone is very strong (the rates of stretching are of the order of 100–1000 s^{-1}). This describes the physical pattern responsible for the formation of the straight thin segment of the electrospinning jets. The liquid stretching by the electrical field in the straight part of the jet weakens, as the jet elongates, to the level of 20–100 s^{-1} according to Refs. [5,7], and the initial longitudinal stresses relax at a distance of about 2–4 cm from the transition zone that connects the modified Taylor cone and the thin segment. Our observations of the transition zone reveal that the straight section of the electrospinning jets is longer at higher voltage because higher initial stresses are generated in the transition zone at higher applied voltages so the straight jet is stabilized for a longer distance. After that (at $x \geq 2$–4 cm), the electrically driven bending instability, characteristic of electrospinning, can set in and dramatic elongation, somewhat similar to the elongation following the modified Taylor cone, occurs initially at rates of about 1000 s^{-1} ([5]). The results also point to an opportunity to build a novel elongational rheometer for semi-dilute and concentrated polymer solutions and melts allowing for stretching rates of the order of 100–1000 s^{-1}. For the 6 wt% aqueous polyethylene oxide solution electrospun at 3–5 kV, the novel elongational rheometer introduced in the present work reveals that the moduli of elasticity are in the range 53–395 Pa, the Rouse relaxation time in the range 3–8 ms and the initial elongational viscosities in the range 100–200 Pa s.

Acknowledgements

We acknowledge the financial support from the National Science Foundation, DMI-0403835-2 (NIRT), NSF subcontract 25-1110-0038-002 (Nebraska DMI-0600733), and a subcontract through Ohio State University, NSF EEC-0425626 (RF 60002999). The Coalescence Filtration Nanomaterials Consortium of the University of Akron provided financial support and an industrial point of view. The authors thank Dr. Daniel Galehouse for the design and construction of a laser velocimeter, and Mr. Steven Roberts for technician support. DHR and TH thank Apogee Technology Inc. for financial support. ALY also acknowledges partial support of this work by the National Science Foundation under Grant NIRT CBET-0609062.

References

[1] Ziabicki A. Fundamentals of fibre formation. London: Wiley; 1976.
[2] Ciferri A, Ward IM, editors. Ultra-high modulus polymers. London: Appl. Sci. Publ.; 1979.
[3] Ziabicki A, Kawai H, editors. High-speed fiber spinning. New York: Wiley; 1985.
[4] Yarin AL. Free liquid jets and films: hydrodynamics and rheology. Harlow, New York: Longman Scientific and Technical, Wiley and Sons; 1993.
[5] Reneker DH, Yarin AL, Fong H, Koombhongse S. Bending instability of electrically charged liquid jets of polymer solutions in electrospinning. J Appl Phys 2000;87:4531–47.
[6] Yarin AL, Koombhongse S, Reneker DH. Bending instability in electrospinning of nanofibers. J Appl Phys 2001;89:3018–26.
[7] Reneker DH, Yarin AL, Zussman E, Xu H. Electrospinning of nanofibers from polymer solutions and melts. Adv Appl Mech 2007;41:43–195.
[8] Yarin AL, Koombhongse S, Reneker DH. Taylor cone and jetting from liquid droplets in electrospinning of nanofibers. J Appl Phys 2001; 90:4836–46.
[9] Feng JJ. Stretching of a straight electrically charged viscoelastic jet. J Non-Newtonian Fluid Mech 2003;116:55–70.
[10] Carroll CP, Joo YL. Electrospinning of viscoelastic Boger fluids: modeling and experiments. Phys Fluids 2006;18:053102.
[11] Hohman MM, Shin M, Rutledge G, Brenner MP. Electrospinning and electrically forced jets II application. Phys Fluids 2001;13:2221–36.
[12] Horning DW, Hendricks CD. Study of electrically driven jet. J Appl Phys 1979;50:2614–7.
[13] Higuera FJ. Stationary viscosity-dominated electrified capillary jets. J Fluid Mech 2006;558:143–52.
[14] Kowalewski TA, Blonski S, Barral S. Experiments and modeling of electrospinning process. Bull Pol Acad Sci 2005;53:385–94.
[15] Gill SJ, Gavis J. Tensile stress in jets of viscoelastic fluids. I. J Polym Sci 1956;20:287–98.
[16] Gill SJ, Gavis J. Tensile stress in jets of viscoelastic fluids. II. J Polym Sci 1956;21:353–62.
[17] Goren SL, Gavis J. Transverse wave motion on a thin capillary jet of a viscoelastic liquid. Phys Fluids 1961;4:575–9.
[18] Bazilevskii AV, Entov VM, Rozhkov AN. Elastic stresses in capillary jets of dilute polymer solutions. Fluid Dyn 1985;20:169–75.
[19] Middleman S, Gavis J. Transverse wave motion on a thin capillary jet of a viscous liquid. Phys Fluids 1965;8:222–9.
[20] Entov VM, Yarin AL. The dynamics of thin liquid jets in air. J Fluid Mech 1984;140:91–111.
[21] Yarin AL. Strong flows of polymeric liquids: 1. Rheological behavior. J Non-Newtonian Fluid Mech 1990;37:113–38.